VAPYRIN-like is required for development of the moss Physcomitrella patens

Ursina Rathgeb, Min Chen, Flavien Buron, Nadja Feddermann, Martine Schorderet, Axelle Raisin, Gabrielle-Yasymi Häberli, Sophie Marc-Martin, Jean Keller, Pierre-Marc Delaux, et al.

© 2020. Published by The Company of Biologists Ltd | Development (2020) 147, dev184762. doi:10.1242/dev.184762

RESEARCH ARTICLE

VAPYRIN-like is required for development of the moss *Physcomitrella patens*

Ursina Rathgeb[1,*], Min Chen[1,*], Flavien Buron[1], Nadja Feddermann[1], Martine Schorderet[1], Axelle Raisin[1], Gabrielle-Yasymi Häberli[1], Sophie Marc-Martin[2], Jean Keller[3], Pierre-Marc Delaux[3], Didier G. Schaefer[2] and Didier Reinhardt[1,‡]

ABSTRACT

The *VAPYRIN* (*VPY*) gene in *Medicago truncatula* and *Petunia hybrida* is required for arbuscular mycorrhizal (AM) symbiosis. The moss *Physcomitrella patens* has a close homolog (*VPY-like*, *VPYL*), although it does not form AM. Here, we explore the phylogeny of *VPY* and *VPYL* in land plants, and study the expression and developmental function of *VPYL* in *P. patens*. We show that *VPYL* is expressed primarily in the protonema, the early filamentous stage of moss development, and later in rhizoids arising from the leafy gametophores and in adult phyllids. Knockout mutants have specific phenotypes in branching of the protonema and in cell division of the leaves (phyllids) in gametophores. The mutants are responsive to auxin and strigolactone, which are involved in regulation of protonemal branching, indicating that hormonal signaling in the mutants is not affected in hormonal signaling. Taken together, these results suggest that *VPYL* exerts negative regulation of protonemal branching and cell division in phyllids. We discuss *VPY* and *VPYL* phylogeny and function in land plants in the context of AM symbiosis in angiosperms and development in the moss.

KEY WORDS: *Physcomitrella patens*, VAPYRIN, Vesicle trafficking, Secretion, Symbiosis

INTRODUCTION

Most plants live in symbiotic associations with fungi or bacteria, which improve their nutrient supply and stress resistance (Oldroyd et al., 2011; Smith and Read, 2008). Symbiotic communication and establishment of the functional symbiosis requires a suite of genes, known as the common symbiosis signaling (CSS) genes, including *SYMBIOSIS RECEPTOR KINASE* (*SYMRK*) and *CALCIUM AND CALMODULIN-DEPENDENT PROTEIN KINASE* (*CCaMK*). *SYMRK* and *CCaMK* are involved in a pathway that mediates perception of symbiotic signals from the cell periphery to the nucleus, where the transcription of hundreds of downstream symbiosis-related genes is induced (Gutjahr and Parniske, 2013). Although most downstream genes have not been functionally characterized, they are thought to be required for intracellular accommodation of the microbial partner and for installation and functioning of the symbiotic interface. This involves containment of the symbiont within a membrane that controls nutrient and signal exchange, and synthesis of the transport proteins that mediate nutrient transfer (Rich et al., 2017; Roth and Paszkowski, 2017; Wang et al., 2017). The transition of nonsymbiotic root cortex cells to symbiotic cells involves major reprogramming of multiple cellular pathways. Central aspects of this transition are repositioning of the nucleus, establishment of an infection structure known as the pre-penetration apparatus (PPA) (Genre et al., 2008) and reorientation of vesicular trafficking towards the symbiotic interface (Pumplin et al., 2012). Although the cellular reprogramming is of central importance for symbiosis, its regulation is poorly understood.

A central element required for intracellular accommodation of arbuscular mycorrhizal (AM) fungi has been identified in forward genetic screens in *Medicago truncatula* and *Petunia hybrida*. It was named VAPYRIN (VPY), because of its two domains: a vesicle-associated membrane protein (VAMP)-associated protein (VAP) domain and an ANKYRIN domain. Both domains are known as protein:protein interaction domains. While the VAP domain is known primarily from vesicle trafficking (Lev et al., 2008), the ANKYRIN domain is special because it occurs in a large range of sizes, from 1 to 24 ankyrin repeats, and it is one of the most common protein domains in eukaryotes (Michaely et al., 2001). In plants, both domains are very common; however, only in VPY are the two domains combined and only VPY has a large ankyrin domain of 11 predicted repeats (Feddermann and Reinhardt, 2011). Such large ankyrin domains are common in animals, in particular in the ankyrin protein, in which the ankyrin repeat was first described. Ankyrins in animals serve as connectors of resident membrane proteins to the spectrin-actin cytoskeleton (Mohler et al., 2002). In plants, the 11-repeat ankyrin domain of VPY is unique (Feddermann et al., 2010; Feddermann and Reinhardt, 2011).

Most land plants have a closely related *VPY-like* gene (*VPYL*) indicative of a duplication. The predicted VPY and VPYL proteins are very similar. They have no transmembrane domain and no peptide signature indicative of a post-translational modification with a membrane anchor; therefore, they might be expected to be localized to the cytoplasm. However, in *M. truncatula* and *P. hybrida*, GFP-tagged VPY and VPYL are localized to small mobile subcellular compartments of unknown function (Feddermann et al., 2010; Liu et al., 2019; Pumplin et al., 2010), known as VPY bodies, which have an identity that includes trans-Golgi network (TGN) and endosomal features (Bapaume et al., 2019). Based on the interaction of VAPYRIN with EXO70I (Zhang et al., 2015) and EXO70H4 (Liu et al., 2019), two components of the exocyst complex, VPY bodies are likely to be involved in the transport of an important cargo in symbiotic cells.

Initial phylogenetic inference using transcriptomic data indicated that *VPY* and *VPYL* are absent from algae, but can be found in most

[1]Department of Biology, University of Fribourg, 1700-Fribourg, Switzerland. [2]Institut de Biologie, Université de Neuchâtel, 2000-Neuchâtel, Switzerland. [3]Laboratoire de Recherche en Sciences Végétales, Université de Toulouse, CNRS, Auzeville, 31326 Castanet Tolosan, France.
*These authors contributed equally to this work

‡Author for correspondence (didier.reinhardt@unifr.ch)

U.R., 0000-0002-2762-0010; P.-M.D., 0000-0002-6211-157X; D.R., 0000-0003-3495-6783

Handling Editor: Ykä Helariutta
Received 20 September 2019; Accepted 19 April 2020

Development (2020) 147, dev184762. doi:10.1242/dev.184762

land plants that engage in symbiosis (Delaux et al., 2015; Feddermann et al., 2010; Pumplin et al., 2010). Angiosperm clades that do not form symbiosis, such as the Brassicaceae and the Amaranthaceae, have lost *VPY* and *VPYL* (Bravo et al., 2016; Delaux et al., 2014; Favre et al., 2014). This indicates that, in angiosperms, the only selection pressure to maintain *VPY* and *VPYL* is symbiosis, indicative of its specific function in symbiosis.

Although the occurrence of *VPY* and *VPYL* in the genomes of angiosperms correlates with the ability to engage in AM (Delaux et al., 2014), this relationship seems less obvious in non-angiosperms. For example, a putative *VPYL* orthologue has been identified in the moss *Physcomitrella patens*, despite the fact that mosses in general, and *P. patens* in particular, are not able to engage in mycorrhizal associations under natural conditions (Wang and Qiu, 2006), although *in vitro* conditions allow for some level of interaction with AM fungi (Hanke and Rensing, 2010). The only moss genus that has been reported to be mycorrhizal, *Takakia* (Wang and Qiu, 2006), is considered a sister clade of all other mosses (Cox, 2018; Volkmar and Knoop, 2010), indicating that the mosses lost mycorrhizal capacity early during their evolution. The maintenance of *VPYL* in the absence of symbiosis suggests that *VPYL* may have nonsymbiotic functions in mosses. Because *VPY* function is restricted to symbiosis, based on the symbiosis-specific *vpy* mutant phenotypes in petunia and *M. truncatula*, the question arises whether *VPYL* in angiosperms has retained such developmental functions, after the duplication and involvement of *VPY* in symbiosis.

To elucidate the origin and function of *VPY*, we established its phylogeny in land plants and investigated *VPYL* function in the nonsymbiotic model plant *P. patens*, which offers excellent molecular genetic tools for exploring gene function, including gene targeting by homologous recombination (Schaefer, 2002). It is therefore an excellent tool for reverse genetic analyses and has become a standard model system for developmental analysis (Prigge and Bezanilla, 2010). *P. patens* spores germinate to form a juvenile protonema that displays a filamentous growth pattern. The leafy gametophores, nonvascular shoots carrying simple leaves (phyllids) formed by a single cell layer, then differentiate by caulinary growth (Kofuji and Hasebe, 2014). These features mean that *P. patens* is an excellent experimental system for the study of cellular aspects of *VPYL* function in a nonsymbiotic context.

RESULTS

Evolution and phylogeny of the VAPYRIN clade in plants

To explore the origin and phylogeny of *VPY* and *VPYL*, we first performed a sequence analysis of the predicted *VPY* homologs in

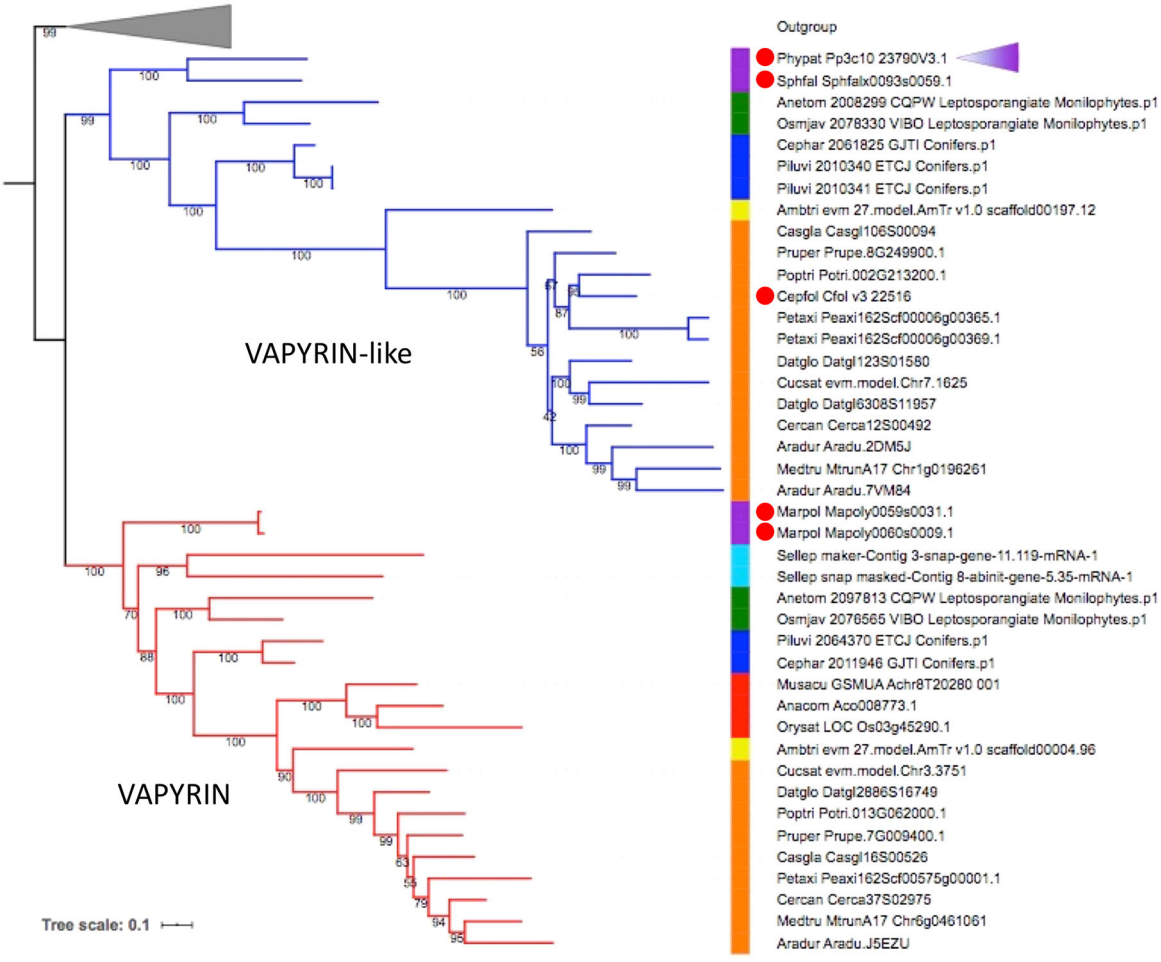

Fig. 1. Phylogenetic tree of the VAPYRIN gene family in selected land plants. Maximum likelihood tree (model JTT+R8) of VAPYRIN (red) and VAPYRIN-like (blue). The tree was rooted using closely related sequences (outgroup, gray triangle). Node supports are indicated by numbers on branches. The colored bar indicates the following clades: purple, bryophytes; cyan, lycophytes; green, monilophytes; blue, gymnosperms; yellow, basal angiosperms; red, monocots; orange, eudicots. The position of the *P. patens* VAPYRIN-like (*VPYL*) sequence is indicated by a purple triangle. Red dots indicate non-mycorrhizal species. See Table S1 and protein sequences in the supplementary Materials and Methods for further information.

Development (2020) 147, dev184762. doi:10.1242/dev.184762

several major land plant taxa, including dicotyledonous and monocotyledonous angiosperms, gymnosperms, ferns, lycophytes and nonvascular representatives of the mosses and liverworts (bryophytes) (Table S1; see protein sequences in the supplementary Materials and Methods). We also included five recently published genomes of streptophyte algae, the closest algal relatives to land plants. The best hits identified in streptophyte algae all lacked either the ankyrin or the VAP/MSP domain, indicating that the VPY/VPYL clade evolved in land plants, as previously suggested on the basis of transcriptomic data (Delaux et al., 2015). Most land plant taxa have at least one *VPY* homolog, and many have a similar *VPYL* gene (Fig. 1) that encodes a protein with a similar predicted domain structure. Based on the overall structure of the phylogenetic tree, *VPY* is likely to have emerged in an early common ancestor of land plants, followed by a duplication event resulting in two paralogous clades (*VPY* and *VPYL*; Fig. 1; Fig. S1). Both clades show strong purifying selection (ω_{VPY}=0.2250; ω_{VPYL}=0.1178), as estimated by comparison of non-synonymous and synonymous nucleotide substitutions (dN/dS ratio, as assessed using the yn00 method), suggesting a conserved biochemical function. Comparing the dN/dS ratio of *P. patens VPYL* with *VPYL* from all other species revealed the same trends (mean, 0.3167733; standard error, 0.02458039). Most taxa retained both paralogues (e.g. dicots, gymnosperms, ferns), but others maintained only *VPY* (monocots, lycophytes, liverworts) or *VPYL* (mosses). On the other hand, many dicots displayed additional gene copies of one or the other paralogue, indicative of additional rounds of duplication, as for instance in the Papilionoideae, the largest subfamily of the Fabaceae, members of which have each at least two *VPY* copies, with the exception of *M. truncatula* that lost one of these recent paralogues (Fig. S2). This duplication probably resulted from an ancestral whole genome duplication that occurred before the radiation of this subfamily (Koenen et al., 2019 preprint).

As observed previously (Delaux et al., 2014; Feddermann et al., 2010; Pumplin et al., 2010), nonsymbiotic angiosperms such as the Brassicaeae (with *Arabidopsis thaliana*) and the Amaranthaceae, as well as the monocot *Zostera marina* lost both *VPY* and *VPYL*, presumably as a consequence of the relaxed selection pressure following the loss of symbiosis in these taxa. This phylogenomic pattern, and the fact that *vpy* mutants in *P. hybrida* and *M. truncatula* have no developmental phenotypes (Feddermann et al., 2010; Murray et al., 2011; Pumplin et al., 2010), suggests that *VPY* (and perhaps *VPYL*) in seed plants is dispensable for plant development and that its function is specific to symbiosis.

Interestingly, the correlation between the presence of *VPY*/*VPYL* and the competence to engage in AM does not hold true in nonvascular plant lineages. The liverwort *Marchantia polymorpha* has lost *VPYL*, but has retained two copies of *VPY* (Fig. 1).

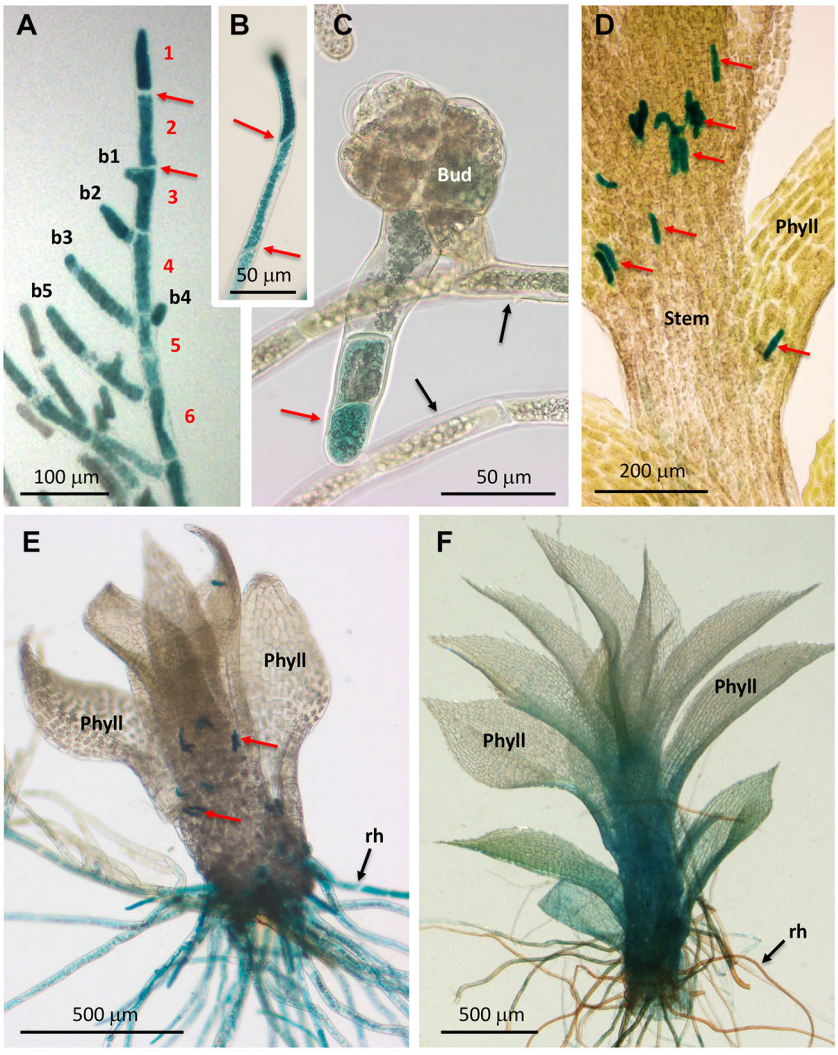

Fig. 2. GUS expression pattern under control of the *P. patens VPYL* promoter. (A-F) Samples of the *pVPYL::GUS* line stained for β-glucuronidase activity. (A) Chloronema with perpendicular cell walls (red arrows). Cells of the main branch are numbered in red (1-6), lateral branches are numbered in black (b1-b5). Older protonemal cells exhibit decreased *VPYL* expression relative to the tip. (B) Caulonema with oblique cell walls (red arrows). (C) Protonema and bud with a young rhizoid (red arrow). Note decreased *VPYL* expression in protonema (black arrows). (D) Gametophore with stem-borne rhizoid initials (red arrows). (E) Young gametophore with five phyllids, developing basal rhizoids and stem-borne rhizoid initials (red arrows). (F) Mature gametophore with >12 phyllids and mature brownish rhizoids. Note increasing expression levels in phyllids. Phyll, phyllids; rh, rhizoids.

Development (2020) 147, dev184762. doi:10.1242/dev.184762

Conversely, the moss *P. patens* has lost *VPY*, but has retained *VPYL* (Phypat Pp3c10 23790V3.1). Interestingly, both these nonvascular plants are nonsymbiotic. This indicates that these *VPY* homologs in nonvascular species have a nonsymbiotic function, which may be related to the ancestral function of the first *VPY* in early embryophytes.

Expression pattern of the *VPYL* gene in *P. patens*

P. patens allows straightforward gene replacement by homologous recombination (Schaefer, 2002); hence, we decided to assess the function of *P. patens VPYL* using this reverse genetic tool. As a first step, we assessed its expression pattern across the different cell types and developmental stages. To assess gene expression with cellular resolution, we chose a promoter-reporter strategy by inserting the bacterial β-glucuronidase (GUS) gene *UidA* downstream of the *VPYL* promoter, thereby leaving about 800 nt of duplicated promoter (5′-TS) sequence of the original *VPYL* promoter (downstream of the GUS insertion cassette) to control the *VPYL* ORF, resulting in the reporter line *pVPYL::GUS* (Fig. S3). This line exhibited no developmental phenotype (compared with the knockout phenotype described below), indicative of normal *VPYL* function, thereby showing that the 800 bp 5′-UTR can be regarded as a fully functional *VPYL* promoter.

At early stages of development, *P. patens* produces filamentous protonemata that grow by tip growth in combination with lateral branching from the apical end of subapical cells (Menand et al., 2007) (Fig. 2A). The protonema consists of two distinct cell types, the photosynthetic chloronemata and the adventitious caulonemata, which mediate rapid radial expansion of the protonema (Menand et al., 2007). *VPYL* expression was consistently high, both in chloronema and caulonema, in particular in the youngest cells at the tip and in young branches (Fig. 2A,B). At later stages of development, *VPYL* expression in the protonema decreased (Fig. 2A), but resumed in the lateral buds that give rise to the gametophores. Remarkably, the main body of the buds showed low expression, whereas *VPYL* was strongly induced in cells at the bottom that develop into rhizoids (Fig. 2C). In developing gametophores, *VPYL* expression was highest in aerial rhizoid initials (Sakakibara et al., 2003) (Fig. 2D) and in growing basal rhizoids (Fig. 2E), whereas it decreased in fully grown rhizoids (Fig. 2F). The stem and the leaf-like structures (phyllids) exhibited low expression at early stages (Fig. 2E); however, at later stages of gametophore development, *VPYL* expression increased from the base of the stem into the phyllids (Fig. 2F). Taken together, these results show that *P. patens VPYL* expression is highest in cell types with a filamentous growth mode (protonema and rhizoids), with lower expression levels in gametophores, in particular in mature phyllids. This global expression pattern is consistent with the pattern revealed in a large scale transcriptomic analysis accessible at the Physcomitrella eFP Browser (http://bar.utoronto.ca/efp_physcomitrella/cgi-bin/efpWeb.cgi) (Ortiz-Ramírez et al., 2016) (Fig. S4).

Phenotypic analysis of *P. patens vpyl* knockout mutants

To explore the function of *VPYL* in *P. patens*, the *VPYL* ORF was deleted by homologous recombination (HR) to generate loss-of-function *vpyl* mutants (Figs S3 and S5). For that purpose, the entire *VPYL* ORF was replaced by a selectable resistance cassette for the antibiotic G418 (Fig. S3). Two independent mutant lines (*ko27* and *ko36*) were identified by PCR genotyping based on the presence of the expected recombined junctions generated by HR, and on the absence of the *VPYL* coding region (Fig. S5B) and the *VPYL* transcript (Fig. S5C). These two knockout lines were used for detailed phenotypic characterization. First, we assessed overall growth of the plants under standard growth conditions on solid BCD agar medium. Overall, mutant plants grew more slowly in diameter and initiated gametophores earlier than the wild type (Fig. 3A,B), whereas development of the protonema was strongly reduced (Fig. 3B). Quantification of colony growth over a time course confirmed the slower expansion growth and the earlier initiation of gametophores in *vpyl* mutants (Fig. 3C-E). Whereas overall colony surface increased more slowly

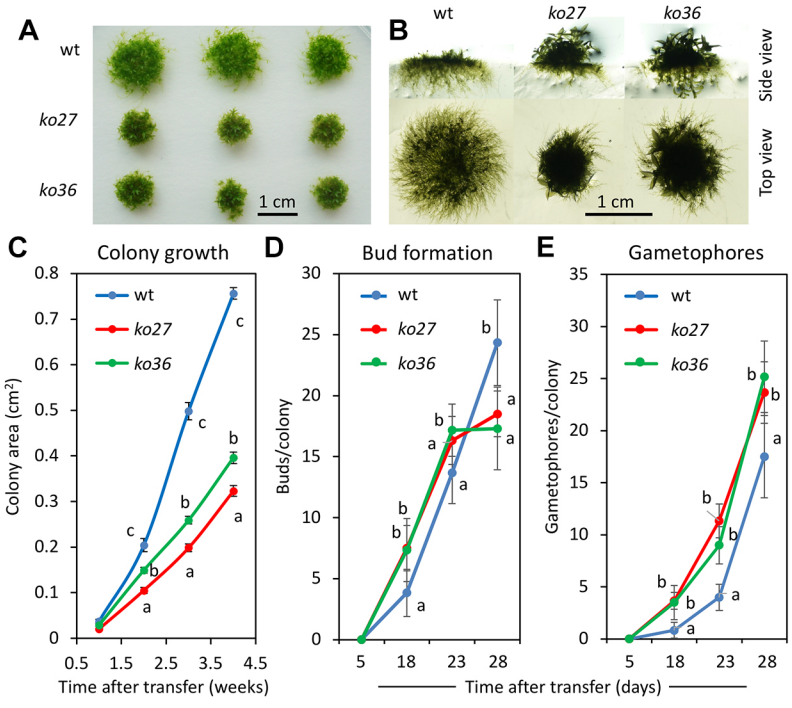

Fig. 3. Global phenotype of *P. patens vpyl* knockout mutants *ko27* and *ko36*. (A) Overall colony growth of wild type (wt) and the two *vpyl* mutants (*ko27*, *ko36*) represented by three replicate plants each after 4 weeks of culture on agar plates with BCD medium. (B) Side view and top view of representative colonies as in A at higher magnification. (C) Plant area growth over a time course of 4 weeks. (D) Bud formation over a time course of 4 weeks. (E) Emergence of gametophores over a time course of 4 weeks. Values represent the mean±s.d. of 15 (C) or 6 (D,E) biological replicates. Different letters indicate significant differences (two-way ANOVA, $P<0.05$). See *P*-values in the supplementary Materials and Methods.

Development (2020) 147, dev184762. doi:10.1242/dev.184762

in the mutants (Fig. 3C), they produced more buds and gametophores (Fig. 3D,E). At the 4 week time point, however, bud formation in the wild type exceeded that in the mutants, presumably as a result of the larger total area covered by the protonema (Fig. 3B) and a concomitant increase in the number of protonemal cells competent for bud formation.

Slower colony expansion in mutants could potentially be a result of retarded transition of protonemata from the slow-growing chloronema cell type to the fast-growing caulonema cell type. Hence, we carried out growth measurements under conditions that favor caulonema development. Initially, the three genotypes were grown on BCD plates with 0.5% glucose for 18 days under low light conditions, then they were transferred to very low unilateral light. Under these conditions, protonemata acquire caulonema identity and grow phototropically towards the dim light source. The directional growth pattern and the synchronized transition from chloronema to caulonema identity allows quantification of caulonemal growth dynamics. At 6 days after initiation of the dark treatment, all three genotypes had initiated caulonemata, which had grown to approximately 2 mm in length (Fig. S6). The mutants had grown slightly longer (difference significant only for *ko27*). These results show that the *vpyl* mutants are not affected in the initiation of caulonemata, nor in their elongation rate.

Closer inspection revealed that the protonemata in mutants produced more branches than in the wild type (Fig. 4A,B). Quantification confirmed that the mutants exhibited a significantly increased average branch number per cell (Fig. 4C), whereas cell length was not affected in the mutants (Fig. S7A,B). Interestingly, branching sometimes occurred in abnormal positions in the mutants (Fig. 4D,F). In the wild type, branches were initiated almost exclusively at the apical end of subapical cells (Fig. 4D,E, arrows), whereas in the mutants lateral branches were often formed in a more proximal position, including the middle of the cells (Fig. 4D,F, blue arrow).

Apart from the site of branch initiation, the length and size distribution of branches in *P. patens vpyl* mutants were also affected (Fig. 5). Normally, lateral branches grow progressively longer after their initiation, resulting in a 'pine-tree' organization of *P. patens* protonemata (Fig. 5A). This results in a clear correlation of branch length with distance from the tip (coefficient of determination R^2=0.78; Fig. 5B). In the *vpyl* mutants *ko27* and *ko36*, this relationship was much less obvious (R^2=0.046 and 0.103, respectively; Fig. 5C,D). This was mainly caused by a generally reduced extension rate of protonemal branches (Fig. 5C-E), but also to a lack of coordination between the position and length of the branches (Fig. 5C,D). Overall branch extension was significantly lower in mutants than in the wild type (Fig. 5E). Log10 transformation of the data set revealed that branch length was log-normally distributed (Fig. S8); hence, statistical analysis was performed on log10-transformed data (Fig. 5E; Fig. S8). Taken together, these data show that the mutants branch more frequently and at illegitimate positions, relative to the wild type, and that the branches develop more slowly after initiation. This can explain the global growth phenotype of the mutants (Fig. 3A,B).

Gametophore phenotype of *P. patens vpyl* mutants

Although gametophores were formed earlier in the mutants, they were macroscopically indistinguishable in their overall morphology. However, closer examination at higher magnification revealed that the cells of the fully mature leaves (phyllids) were smaller in the mutants relative to the wild type (Fig. 6A-C). On average, mutant cells had approximately half the length of wild-type cells (Fig. 6D).

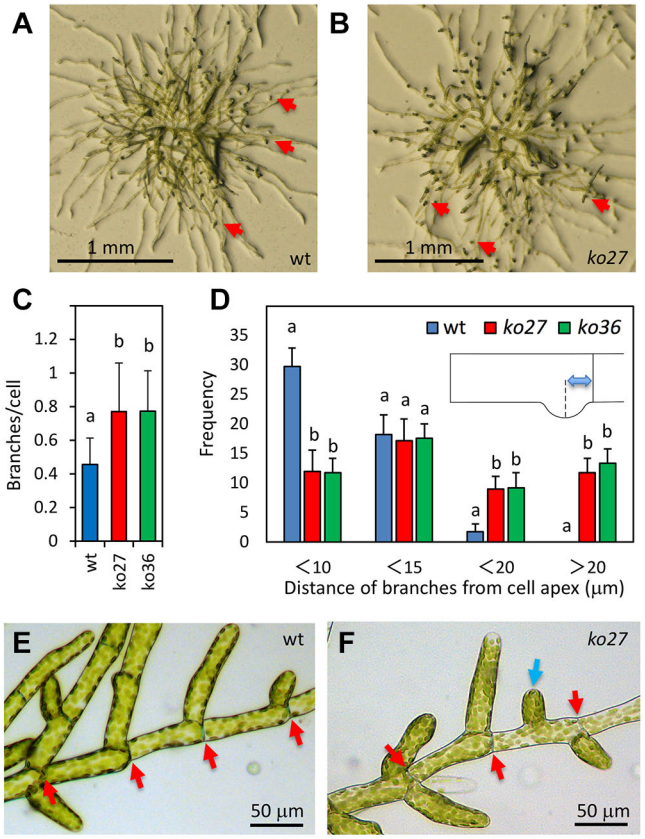

Fig. 4. Branching phenotype of *P. patens vpyl* knockout mutants *ko27* and *ko36*. (A) Protonemal appearance of a young wild-type plant. Arrows indicate lateral branches that grow into the air. (B) As in A with a plant of *ko27*. (C) Average branching index for the first five cells of protonemal files in wild type, *ko27* and *ko36* (*n*=100 per genotype). (D) Distance of branching site from the apical end of cells in protonemal files in wild type, *ko27* and *ko36* (compare with E,F). For each branch, its distance from the upper end of the protonemal cell (see schematic inset) was measured. Only the first five cells in a protonemal file were considered (*n*=125 per genotype). (E) Branching pattern in the wild type. Red arrows indicate the apical end of the cells. (F) Branching pattern in *ko27*. Red arrows indicate the apical end of the cells. Blue arrow indicates an illegitimate branch site in the middle of a cell. Values represent the mean+s.d. Different letters indicate significant differences (two-way ANOVA, P<0.05). See *P*-values in the supplementary Materials and Methods.

This was true for cells close to the midrib (inner), cells in the middle of the lamina (middle), and cells at the leaf edge (outer) (Fig. 6D). Interestingly, cell width was indistinguishable between mutants and wild type (Fig. 6E). Quantification of overall phyllid dimensions showed that *vpyl* mutants and the wild type had very similar phyllid sizes (Fig. 6F). Although mutants exhibited a small but significant reduction in phyllid length, the small difference of 8.7% does not compare with the approximately 50% reduction in cell length. Hence, *P. patens vpyl* mutant phyllids have more, but shorter, cells than the wild type, suggesting that the mutants undergo additional rounds of cell division compared with the wild type.

Hormones rescue the protonemal phenotype of *P. patens vpyl* mutants

Branching of protonema in *P. patens* is known to be under hormonal control (Knight et al., 2009). Strigolactone inhibits branching (Proust et al., 2011), whereas auxin causes a combination of changed identity (from chloronema to caulonema) and reduced branching (Thelander et al., 2018). To test whether the mechanism

Development (2020) 147, dev184762. doi:10.1242/dev.184762

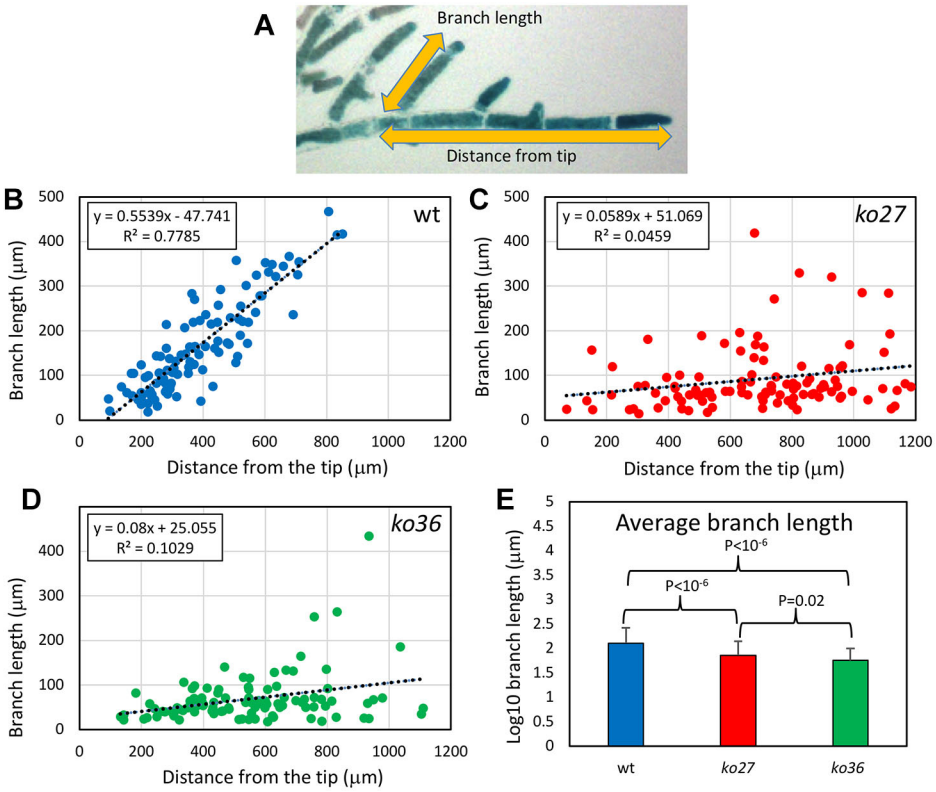

Fig. 5. Branch length distribution in wild type and knockout mutants *ko27* and *ko36*. (A) Branch length distribution is defined as the length of branches in dependence of their distance from the tip of the protonemal file. (B) Branch length distribution in the wild type (wt). (C) Branch length distribution in *ko27*. (D) Branch length distribution in *ko36*. (E) Branch length in wild type, *ko27* and *ko36*. Values represent the mean+s.d. (*n*=105). Branch length distribution was log10-normally distributed (see Fig. S8). Therefore, values were log10 transformed followed by two-way ANOVA and Tukey post hoc tests.

involving *VPYL* interacts with hormonal regulation, we exposed mutants and wild-type protonemata to the synthetic strigolactone GR24 and to the auxin 1-naphthylacetic acid (NAA) at concentrations of 1-10 µM. These concentrations did not significantly alter overall colony growth of *P. patens*, indicating that such concentrations are within the physiological range (Fig. S9A). A partial loss of chlorophyll in response to NAA (Fig. S9A) is consistent with the onset of the transition from chloronema to caulonema identity in response to auxin treatment. Quantification of protonemal branching revealed a strong inhibitory effect of both hormones on branch numbers (Fig. 7). The strigolactone GR24, as well as the auxins NAA and indole-3-acetic acid (IAA) all significantly inhibited protonemal branching, both in the wild type and in the two *vpyl* knockout lines (Fig. 7). These results

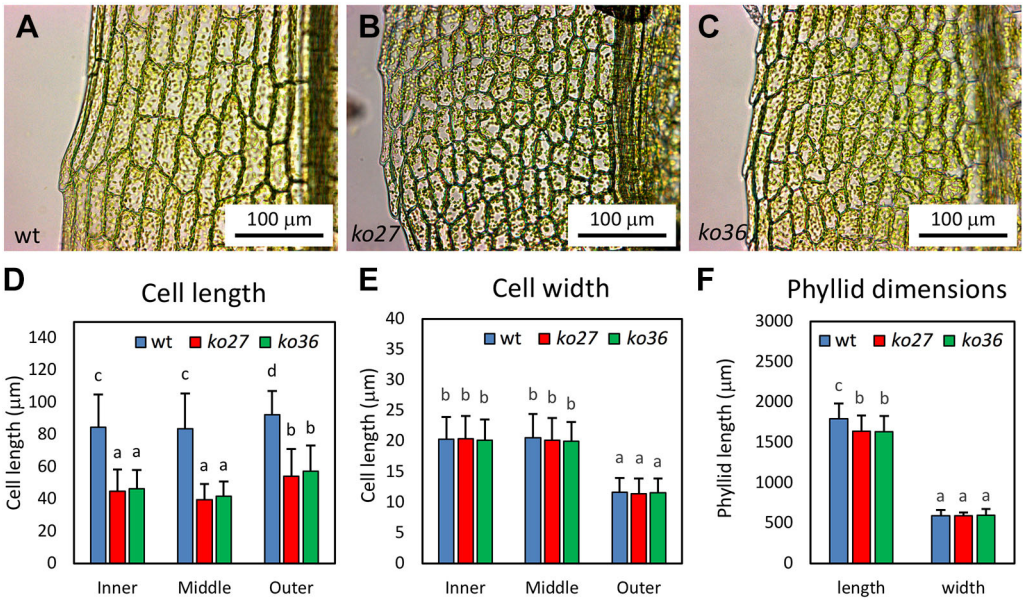

Fig. 6. Phyllid phenotype of *P. patens vpyl* knockout mutants *ko27* and *ko36*. (A) Representative phyllid of a wild-type gametophore. (B) Representative phyllid of a *ko27* gametophore. (C) Representative phyllid of a *ko36* gametophore. (D) Average phyllid cell length in the wild type, *ko27* and *ko36* (*n*=100). (E) Average phyllid cell width in the wild type, *ko27* and *ko36* (*n*=100). (F) Overall phyllid length and width in the wild type, *ko27* and *ko36* (*n*=20). Bars represent the mean+s.d. Different letters indicate significant differences (two-way ANOVA, *P*<0.05). See *P*-values in the supplementary Materials and Methods.

Development (2020) 147, dev184762. doi:10.1242/dev.184762

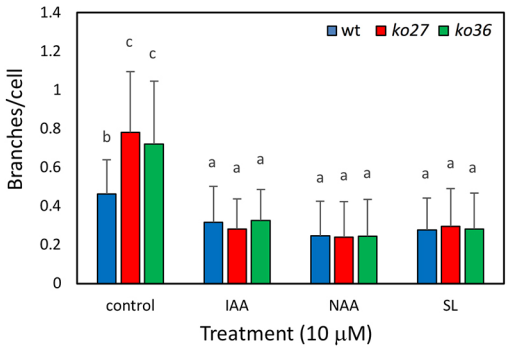

Fig. 7. Hormone-dependent reversal of the branching phenotype in *ko27*, and *ko36*. Average branch number per cell was measured as in Fig. 4C in the wild type, *ko27* and *ko36* in the presence of 10 µM of the auxins NAA and IAA, or of the strigolactone GR24 (SL). Error bars represent the mean+s.d. (*n*=100). Different letters indicate significant differences (two-way ANOVA, $P<0.05$). See *P*-values in the supplementary Materials and Methods.

indicate that the *vpyl* phenotype is not caused by insensitivity to the negative regulators of protonemal branching, SL and auxin. Quantification of chloronemal and caulonemal cells by measuring cell wall angles of the first four cells in protonemal files showed that the material shown in Fig. 7 consisted mainly of chloronemal cells (angle of the wall between successive cells 80-90°; compare with Fig. 2A). However, a gradual shift to smaller angles towards the protonemal tip (first cell) was observed after treatment with IAA (Fig. S9B, arrows), consistent with a gradual transition from chloronemal to caulonemal identity. This auxin-induced developmental response was similar in the wild type and in *vpyl* mutants (Fig. S9B), indicating that auxin-inducible initiation of the transition to caulonemal identity is not compromised in *vpyl* mutants. Taken together, these results suggest that *P. patens vpyl* mutants are not affected in their responses to SL and auxin.

Subcellular localization of *P. patens* VPYL protein

To assess the subcellular localization in *P. patens*, the *VPYL* gene was fused in frame with the fluorescent protein Citrine under the control of the constitutive promoter of the gene encoding elongation factor 1-α (*EF1a*), resulting in *pEF1a::Citrine-VPYL*. This construct was inserted by homologous recombination at the *P. patens* intergenic1 (*PIG1*) locus, which has been shown to be a suitable site for transformation because it does not cause mutant phenotypes upon disruption (Okano et al., 2009). Thus, the *PIG1* locus can serve as a recipient site for gene knock-ins without interfering with development of the moss.

In protonemal cells, Citrine-VPYL exhibited pronounced localization to small subcellular compartments (Fig. 8), apart from a weaker signal in the cytoplasm and nuclei. The subcellular localization to small compartments is reminiscent of the VPY bodies observed in *P. hybrida*, *M. truncatula*, and *Nicotiana benthamiana* (Bapaume et al., 2019; Feddermann et al., 2010; Liu et al., 2019; Pumplin et al., 2010). In analogy to the structures characterized in tobacco (Bapaume et al., 2019), we refer to these structures as VPYL bodies. As in the case of *M. truncatula* (Liu et al., 2019), these compartments were most prominent in areas that are rich in cytoplasm, such as around the nuclei (Fig. 8A). In contrast, free fluorescent protein expressed from a heat-inducible Cerulean construct inserted at the PIG1 site, showed a general cytoplasmic signal that was just excluded from the chloroplasts and the vacuole (Fig. 8A, inset). Strong Citrine-VPYL signal was also observed along the plasma membrane of adjacent protonemal cells

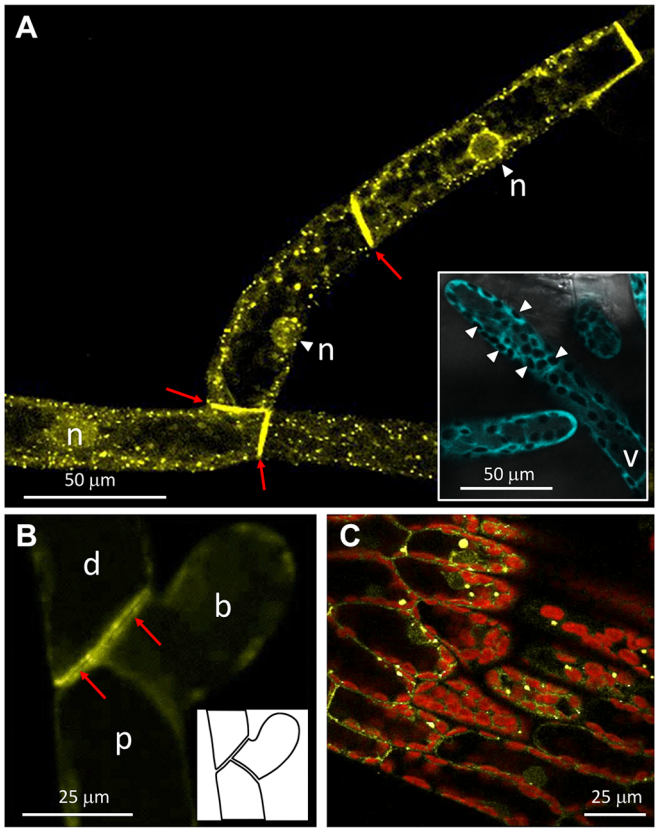

Fig. 8. Subcellular localization of Citrine-tagged VPYL in *P. patens*. (A) Protonemal cell file with nuclei in the focal plane expressing N-terminally tagged Citrine-VPYL under control of the *P. patens* elongation factor 1-α promoter. Note many Citrine-labeled VPYL bodies and accumulation of signal at cell boundaries (arrows). Inset: Free Cerulean is localized throughout the cytoplasm, but excluded from the vacuole and chloroplasts (arrowheads). (B) Localization of Citrine-VPYL in three adjacent protonemal cells, including a distal cell, proximal cell and an early branch. Signal was deliberately kept low to reveal details of the cell boundaries (arrows). Inset shows cellular context. (C) Citrine-labeled VPYL bodies in phyllid cells. Note chlorophyll autofluorescence of chloroplasts (red). b, early branch; d, distal cell; n, nucleus; p, proximal cell; v, vacuole.

next to their shared cell wall (Fig. 8B), at sides where actin also accumulates (Vidali et al., 2009). As in protonemal cells, a subcellular localization to punctate objects was found in phyllids, although in this case the fluorescent compartments were slightly larger and more heterogenous in size than in the protonema (Fig. 8C).

DISCUSSION

Origin, evolution and expression pattern of the VAPYRIN gene family

The small VAPYRIN gene family (including *VPY*, *VPYL* and additional copies thereof) occurs in most land plants. Based on our phylogenetic analysis, the ancestral *VPY* gene emerged at the base of the embryophytes, probably via fusion of the ankyrin domain with the MSP domain, and underwent early duplication. Both copies, *VPY* and *VPYL*, were retained in most angiosperm clades, except in those that lost the capability to engage in AM symbiosis. This phylogenetic signature, and the fact that *vpy* mutants in petunia and *M. truncatula* have no developmental phenotypes, suggests that *VPY* has only symbiosis-related functions. However, the finding that some nonsymbiotic mosses and liverworts have retained *VPY* or

Development (2020) 147, dev184762. doi:10.1242/dev.184762

VPYL (Fig. 1; Fig. S1) indicates that it has nonsymbiotic functions in nonvascular plants. The developmental phenotype of *P. patens vpyl* mutants is consistent with this assumption.

The fact that *vpy* mutants in petunia and *M. truncatula* have a strong symbiosis-defective phenotype indicates that there can be only limited redundancy between *VPY* and *VPYL*, if any, and that the function of the latter in angiosperms remains to be found. In this context, it is interesting that, according to the *M. truncatula* Gene Expression Atlas (https://mtgea.noble.org/v3/), the *M. truncatula VPY* gene is expressed almost exclusively in roots (Fig. S10A) and is highly responsive to nodulation (Fig. S10B), mycorrhizal infection (Fig. S10C), nod factor and rhizobia in root hairs (Fig. S10C). In contrast, *M. truncatula VPYL* has a broader expression domain, including shoot tissues (Fig. S10A), and is not influenced by symbiotic status or symbiotic signals in the roots (Fig. S10B,C). This indicates that *VPYL* has nonsymbiotic functions in *M. truncatula* (and presumably in other angiosperms) that remain to be discovered.

Expression pattern and developmental function of *VPYL* in *P. patens*

Our analysis using a *pVPYL::GUS* construct revealed that the *VPYL* promoter is most active in protonema (caulonema and chloronema) and in young rhizoids (Fig. 2). The common feature of these cell types is their growth mode, which is restricted to tip growth as in the root hairs and pollen tubes of angiosperms. The high expression of *VPYL* at early stages of development in these cell types (protonemal tip cells; rhizoid initials) could indicate that *VPYL* is involved in tip growth. However, the fact that *P. patens vpyl* knockout mutants had no phenotype in tip growth or protonemal cell size (Fig. S7) indicates that the role of *VPYL* in the protonema of *P. patens* is not in cell growth or cell division. Because *P. patens vpyl* mutants show excessive and ectopic branching (Fig. 4), *VPYL* may be involved in the determination of branch sites, thereby influencing protonemal patterning. The initial acceleration of gametophore formation in *vpyl* knockout mutants (Fig. 3) seems at first to concern a different aspect of moss development. However, the buds that give rise to gametophores differentiate from protonemal side branch initials, which subsequently undergo a specific cell division pattern to generate a three-dimensional leafy shoot (Moody, 2019). Hence, the common aspect of all these phenotypic traits in *vpyl* mutants is increased protonemal branching. Hence, *P. patens VPYL* is a determinant of branch site selection and limits excessive branching, thereby controlling protonemal patterning.

Uncoupling of phyllid size and cell size in *vpyl* mutants

A striking aspect of the *P. patens vpyl* knockout phenotype was decreased cell length in phyllids, whereas cell width and total phyllid size was almost normal (Fig. 6). This suggests that phyllid size and cell size are controlled independently. Final organ size is defined by a combination of expansion growth and the cell cycle (Hepworth and Lenhard, 2014). Mechanistically, the two processes can proceed independently; however, cell division is coordinated with expansion in such a way that cell size remains nearly constant at early stages of organ growth, whereas cell division ceases at later stages and the organ reaches its final size and shape by cell expansion. Experiments on tobacco mutants with a dominant negative version of a cell cycle regulator showed that normal organ shape can be attained with fewer (but larger) cells (Hemerly et al., 1995); thus, organ growth and cell division are separable to a certain degree. The opposite phenotype in *P. patens vpyl* mutants (normal leaf size with smaller cells) reflects either increased cell cycle activity or decreased cell diffuse growth in the absence of *VPYL*, whereas the determinants of phyllid size control organ growth independently of cell size and cell number. Strikingly, mutation of *VPYL* only affects one cell dimension (length), indicating that *P. patens VPYL* function in cell division control has a polar component.

Cellular function of VPYL in *P. patens*

An important element in all tip-growing cells is the cytoskeleton (Bascom et al., 2018). In pollen tubes and root hairs, as well as in moss protonemata (Wu et al., 2018), the cytoskeleton is thought to mediate the vesicle transport required for cell wall extension at the tip (Bascom et al., 2018). Although the role of the cytoskeleton in tip growth is well established, its role in protonemal branching is less clear. Mutants in actin-related genes in *P. patens* show a more severe and pleiotropic phenotype than *vpyl* mutants (Finka et al., 2008; Harries et al., 2005; Perroud and Quatrano, 2008). More informative are mutants in myosin VIII genes, which encode motor proteins that move along actin strands. A mutant defective in all five myosin VIII genes (ΔmyoABCDE) of *P. patens* shares several striking similarities in its developmental phenotype with *P. patens vpyl* mutants (Wu et al., 2018, 2011). In particular, ΔmyoABCDE exhibits increased protonemal branching, illegitimate branching sites, uneven distribution of branch length and accelerated gametophore formation. It is interesting to see such similarities to the *vpyl* phenotype because the motility and function of VPYL bodies is probably related to motor proteins such as myosins.

Functional parallels of VPY and VPYL in symbiosis and cell branching

In the angiosperms *P. hybrida*, *M. truncatula* and *N. benthamiana*, GFP-tagged VPY localizes to small subcellular compartments (VPY bodies) with endosomal identity (Bapaume et al., 2019; Feddermann et al., 2010; Pumplin et al., 2010). A similar subcellular localization was found in *P. patens* (Fig. 8). Could this indicate commonalities in the cellular events associated with endosymbiosis and with protonemal branching? One common aspect of both phenomena is the accumulation of large amounts of cytoplasmic constituents and organelles, both in the accommodation of an intracellular microbe and in the establishment of a new tip-growing branch. Cellular events in the host associated with microbial infection and accommodation have been compared with cytokinesis because of overlapping gene expression patterns (Breakspear et al., 2014) and prominent similarities in assembly of the phragmoplast and infection structures such as the PPA (Genre et al., 2012). In addition, symbiosis requires assembly of the large amounts of membrane material that surrounds the growing tips of arbuscules (in AM) and the invading or accommodated rhizobia (in RNS). With their trans-Golgi and endosomal identities (Bapaume et al., 2019), and given the interaction with exocyst components (Liu et al., 2019; Zhang et al., 2015), VPY bodies may well play an important role in these processes.

An additional striking parallel is the involvement of nuclear repositioning in all three processes: protonemal branching is associated with migration of the nucleus to an apical position next to the branch site (Doonan et al., 1986; Jensen, 1981; Schmiedel and Schnepf, 1979) (Fig. S11A). On the other hand, fungal and bacterial accommodation in AM and RNS is guided by the nucleus, which dictates the trajectories of the PPA (Genre et al., 2008, 2005) and infection thread, respectively (Fournier et al., 2008) (Fig. S11B,C). A unifying interpretation of these phenomena could be a scenario in which new foci of tip growth are initiated by nuclear positioning and assembly of a tip-growing

Development (2020) 147, dev184762. doi:10.1242/dev.184762

machinery, after which the newly established tip grows outward (in branching moss protonema) or inward (in PPA and infection thread). It remains to be explored how VPY and VPYL impinge on these processes to promote accommodation of endosymbionts and to limit protonemal branching.

MATERIALS AND METHODS

Phylogenetic analysis

VAPYRIN homologs were searched against a custom genome database of 77 plant species from the SymDB database (Radhakrishnan et al., 2020) covering the main orders of plant lineages from bryophytes to angiosperms. Additionally, data from the 1KP project (Matasci et al., 2014) were added to improve coverage of the gymnosperm and monilophyte lineages (Table S1; see protein sequences in the supplementary Materials and Methods). Searches were performed with the tBLASTn algorithm v2.9.0+ (Camacho et al., 2009) with an e-value threshold of 1e-10 and the protein sequence of VAPYRIN from the model legume *Medicago truncatula* as query. Obtained coding sequences were aligned with MAFFT v7.407 (Katoh and Standley, 2013) with default parameters. The resulting alignment was cleaned by removing all positions with more than 20% of gaps using trimAl v1.2 (Capella-Gutierrez et al., 2009). The clean alignment was used as matrix for subsequent phylogenetic analysis by maximum likelihood using IQ-TREE v1.6.7 (Nguyen et al., 2015). First, the best-fitted evolutionary model was tested using ModelFinder (Kalyaanamoorthy et al., 2017) according to the Bayesian Information Criteria. Maximum likelihood analysis was then performed with 10,000 replicates of UltraFast Bootstraps (Hoang et al., 2018) to test the branch support. The resulting phylogeny revealed three main clades, with two paralogous groups corresponding to VAPYRIN and VAPYRIN-like. Sequences from the third clade were used as an outgroup. From this first analysis, three subsets were extracted and subjected to detailed phylogenetic analysis: the clade VAPYRIN/VAPYRIN-like with all sequences (Fig. S1), the VAPYRIN/VAPYRIN-like clade with only representative species of plants orders (for readability reasons) (Fig. 1) and the Fabaceae VAPYRIN clade (Fig. S2). In all cases, the obtained topologies were similar, with slight differences in the positions of some terminal branches. Each of the subsequent phylogenetic analyses was performed on both protein and protein-coding sequences (with a gap trimming threshold set as 50% for the protein-coding sequences). Similar results were obtained and the tree with the best resolution was selected (the only difference between trees based on proteins and coding sequences was the resolution of some terminal branches). Proteins were aligned using MUSCLE v3.8.31 (Edgar, 2004) with the default parameters. The alignment was then subjected to maximum likelihood analysis following the procedure described above.

Trees were visualized and annotated throughout the Interactive Tree Of Life (iTOL) platform v4.3.3 (Letunic and Bork, 2019).

Analysis of selection signature

Analysis of the selective constraint acting on the *VPY* and *VPYL* genes was conducted using the PAML4.9j package (10.1093/molbev/msm088). Protein alignments from phylogenic analysis were used, and sequences with more than 50% of gaps removed before realignment of sequences using MUSCLE. Obtained alignments were used as templates to generate the codon alignment using the PAL2NAL Perl script (10.1093/nar/gkl315) with the option to remove all gapped position for subsequent analysis. The resulting alignment of 166 sites was subjected to a dN/dS analysis using the YN00 method from the PAML package (10.1093/molbev/msm088; 10.1093/oxfordjournals.molbev.a026236).

Plant material, culture conditions and protoplast transformation

P. patens (standard lab strain Gransden) was grown under sterile conditions on 0.8% agar containing BCD medium in 9 cm Petri dishes as described (Ashton and Cove, 1977; Ashton et al., 1979; Trouiller et al., 2006). Growth chamber conditions were adjusted to a day:night photoperiod of 16:8 h (25/22°C) at a photon fluence rate of approximately 50 µmol/m^2/s. *P. patens* was routinely grown on cellophane discs except for analysis of total colony growth (Fig. 3).

For detailed microscopic analysis, the moss was grown between two cellophane sheets (sandwich method). In the case of hormonal treatments, *P. patens* was first grown on BCD medium for one week before transferring the cellophane sandwich to a BCD plate with IAA (Sigma-Aldrich), NAA (Fluka), or GR24 (Strigolab) at the indicated concentrations for one week. Hormones were diluted in 40 µl of solvent (36 µl ethanol and 4 µl hormonal stock in DMSO) in Petri plates before adding 40 ml BCD medium. Protoplast isolation and polyethylene glycol-mediated transformation of *P. patens* protoplasts were performed as previously described (Schaefer and Zrÿd, 1997; Trouiller et al., 2006).

Cloning of transformation vectors

The knockout vector p*VPYL*-KO was constructed in the vector *pBNRF* that carries an *nptII* expression cassette conferring G-418 resistance (Schaefer et al., 2010). Two 800 bp targeting sequences (5′-TS and 3′-TS) covering the sequences located immediately up- and downstream of the *P. patens VPYL* ORF were amplified by PCR using primers ko-5′F and ko-5′R, and ko-3′F and ko-3′R, respectively (see primer list in the supplementary Materials and Methods). The amplified fragments were cloned in *pBNRF* to generate the replacement vector p*VPYL*-KO (see vector constructs in the supplementary Materials and Methods). For transformation, 15 µg of vector DNA was linearized with *Sal*1 and *Mlu*1, precipitated with ethanol and resuspended in sterile water. Homologous recombination on both TSs resulted in the replacement of the *P. patens VPYL* ORF by the *nptII* resistance gene (Fig. S3).

A GUS reporter line was generated by insertion of the *UidA* gene, which encodes bacterial β-glucuronidase (GUS), under the control of the full-length *P. patens VPYL* promoter. First, a 1.6 kb fragment containing the coding sequence of β-glucuronidase and the *NOS*-terminator, including an *Xho*I restriction site on each side, was amplified by PCR from the plasmid *pMDC163* (Curtis and Grossniklaus, 2003) using primers #19fw and #20rev (see the primer list in the supplementary Materials and Methods). This fragment was inserted between the 5′-TS and the resistance marker in the knockout vector *VPYL*-KO. For transformation, 15 µg vector DNA was linearized only with *Sal*1, precipitated with ethanol, and resuspended in sterile water. This construct was introduced into the *P. patens* genome at the *VPYL* locus by homologous recombination only at the 5′-TS, resulting in insertion of the linearized vector, instead of replacement of the *VPYL* ORF (Fig. S3).

For analysis of subcellular localization, an N-terminal Citrine-VPYL fusion was built in the gateway-compatible destination vector pOYG1 (http://moss.nibb.ac.jp/protocol.html) designed for insertion at the *PIG1* locus. The *PIG1* locus is considered silent and therefore suited for insertion (Okano et al., 2009). The *VPYL* ORF including the stop codon was amplified by PCR and integrated into the pENTRTM/D-TOPO vector, followed by an LR recombination reaction with the preformed Gateway-compatible transformation vector pOYG1. The *VPYL* ORF was thereby fused in frame to Citrine at its N-terminal end. Expression of the fusion protein is under control of the strong constitutive *EF1a* promoter. For transformation, 15 µg vector DNA was linearized with *Pme*I, precipitated with ethanol, and resuspended in sterile water. As a cytoplasmic control, heat shock-inducible free Cerulean (pPIG1HCG) (Aoyama et al., 2012) was used 24 h after heat shock at 38°C for 1 h.

β-Glucuronidase assay

GUS activity was determined by staining in the following staining solution: 0.5 mg/ml 5-bromo-4-chloro-3-indolyl β-D-glucuronide cyclohexylammonium salt (X-Gluc) in 125 mM sodium phosphate buffer (pH 7.5), 0.2 mM EDTA, 0.02% NaN3, 0.1% Triton-X-100, 5 mM ferricyanide and 5 mM ferrocyanide. Staining was performed for 3 h (Fig. 2B,C,F) or overnight (Fig. 2A,D,E) at 37°C. Chlorophyll was removed by consecutive immersion in 50, 75 and 100% ethanol.

Microscopy

For detailed phenotypic characterization, moss grown in a cellophane sandwich was excised from Petri plates with care to avoid shifts of the protonema between the cellophane layers. These samples were then

mounted with water on object slides and images acquired with an Axiocam color CCD camera (Zeiss Axiophot I) operated by AxioVision 2.05 software (Zeiss) and mounted on a Leica DMR microscope. Confocal analysis was performed on a Leica SP5 with an argon laser (458, 476, 488 and 514 nm) and a helium-neon laser (543 nm) using the respective laser for Citrine and chlorophyll autofluorescence. Pictures were edited with the Leica LAS AF Lite software and ImageJ.

Phenotypic analysis of *P. patens vpyl* mutants

For quantitative analysis of colony growth, normalized tissue suspensions of *P. patens* wild type, *ko27* and *ko36* were pre-grown for 1 week on BCD medium overlaid with cellophane. At the start of the experiment, protonemal fragments of about 1 mm in diameter were transferred to fresh BCD plates (without cellophane) as triplets and grown for an additional 4 weeks under standard conditions. Colony expansion was determined by analyzing scans of the bottom of each Petri dish. The area of expansion was measured using the Particle Analysis function of ImageJ software on 8-bit Image type pictures with an auto-adjusted threshold. Numbers of buds and gametophores present in each moss colony were counted by eye through a binocular (Leica MZ-FLIII) after dissection.

For quantification of caulonemal growth, pre-grown protonemata were aligned in cellophane sandwiches on BCD supplemented with 5 mM ammonium tartrate and 0.5% glucose. About three-quarters of each plate surface was wrapped with aluminum foil to initiate directional phototropic growth perpendicular to the aligned protonemata for 18 days. Subsequently, plates were wrapped with black plastic and aluminum foil to leave only a narrow light window of ca. 1 cm diameter, towards which the directionally growing protonemata were oriented. After 6 days of further culture, all protonemata had undergone transition to caulonemal identity. The length of caulonemata was determined from pictures acquired with a Nikon Digital Sight DS-U1 camera mounted an a binocular dissection microscope (Leica MZ-FLIII). For detailed analysis of branch number, branch distribution, average branch length and branch position, *P. patens* wild type, *ko27* and *ko36* were grown under standard conditions (see above) in cellophane sandwiches. Approximately 100 randomly chosen cells or branches were analyzed per treatment, as indicated in the figure legends. Phyllid analysis was performed with fully grown leaves of gametophores after 4 weeks of culture under standard conditions without cellophane. At least five different gametophores were chosen per genotype to measure the dimensions of 20 phyllids or 100 cells per genotype. For cell length measurements, the protonema was stained with Calcofluor White as described (Kofuji et al., 2018) to reveal cell walls and the samples analyzed by confocal analysis. All experiments were repeated at least twice with similar results.

Genotyping

Genomic DNA was isolated by extraction with 20 mM Tris HCl (pH 7.5), 250 mM NaCl, 25 mM EDTA, 0.5% (w/v) SDS and 10 mM β-mercaptoethanol. Extracts were cleared by centrifugation (10 min, 15,000 ***g***) and precipitated with isopropanol. DNA was recovered by centrifugation (10 min, 15,000 ***g*** and washed with 75% ethanol. Genotyping was performed by PCR with the primers listed in the supplementary Materials and Methods (see also Fig. S3).

Gene expression analysis

RNA from protonemal cultures was extracted employing the NucleoSpin RNA Plant Kit (Macherey-Nagel). RNA was reverse transcribed with iScript cDNA Synthesis Kit (BioRad). Quantitative real-time RT-PCR (qRT-PCR) was carried out with primers #51f and #52r (see primer list in the supplementary Materials and Methods) using the qPCR SYBRGreen master mix (ThermoScientific, http://www.thermo.com) in a Rotorgene thermocycler (Corbett Life Science). The PCR conditions included an initial denaturation cycle for 15 min at 95°C, followed by 40 cycles of denaturation for 15 s at 95°C, annealing for 20 s at 60°C and extension for 20 s at 72°C, followed by a final extension for 5 min at 72°C. qPCR analysis was performed with *P. patens TUA1* (GenBank Accession Number AB096718.1) as reference gene (see primer list in the supplementary Materials and Methods). Relative gene expression values were calculated using the ΔΔCt method (Pfaffl, 2001).

Acknowledgements

We thank Guillaume Gouzerh and Noémie Fahr for confocal microscopy, Mitsuyasu Hasebe (NIBB Okasaki, Japan) for providing us with the cloning vectors pOYG1 and pPIG1HCG, and Chiara Pollheimer for assistance in phenotypic analysis. Special thanks go to Rudolf Rohr for help with statistical analysis.

Competing interests

The authors declare no competing or financial interests.

Author contributions

Conceptualization: D.R., D.G.S., P.-M.D.; Methodology: U.R., M.C., N.F., M.S., J.K., P.-M.D., D.G.S., D.R.; Software: J.K.; Validation: U.R., D.G.S.; Formal analysis: U.R., M.C., F.B., N.F., D.G.S.; Investigation: D.R., U.R., N.F., M.S., A.R., S.M., G.-Y.H., J.K., P.-M.D., D.G.S.; Resources: P.-M.D., D.G.S.; Data curation: U.R., F.B., J.K., P.-M.D.; Writing - original draft: D.R., D.G.S.; Writing - review & editing: D.R., U.R., M.C., J.K., D.G.S.; Visualization: D.R., U.R., M.C., F.B., M.S.; Supervision: D.R., D.G.S.; Project administration: D.R.; Funding acquisition: D.R.

Funding

This work was supported by the Schweizerischer Nationalfonds zur Förderung der Wissenschaftlichen Forschung to D.R. (31003A-169732).

Data availability

The *P. patens VPYL* gene sequence can be accessed at GenBank: MN971578TS.

Supplementary information

Supplementary information available online at
http://dev.biologists.org/lookup/doi/10.1242/dev.184762.supplemental

Peer review history

The peer review history is available online at
https://dev.biologists.org/lookup/doi/10.1242/dev.184762.reviewer-comments.pdf

References

Aoyama, T., Hiwatashi, Y., Shigyo, M., Kofuji, R., Kubo, M., Ito, M. and Hasebe, M. (2012). AP2-type transcription factors determine stem cell identity in the moss *Physcomitrella patens*. *Development* **139**, 3120-3129. doi:10.1242/dev.076091

Ashton, N. W. and Cove, D. J. (1977). The Isolation and preliminary characterisation of auxotrophic and analogue-resistant mutants of the moss, *Physcomitrella patens*. *Mol. Gen. Genet.* **154**, 87-95. doi:10.1007/BF00265581

Ashton, N. W., Grimsley, N. H. and Cove, D. J. (1979). Analysis of gametophytic development in the moss, *Physcomitrella patens*, using auxin and cytokinin resistant mutants. *Planta* **144**, 427-435. doi:10.1007/BF00380118

Bapaume, L., Laukamm, S., Darbon, G., Monney, C., Meyenhofer, F., Feddermann, N., Chen, M. and Reinhardt, D. (2019). VAPYRIN marks an endosomal trafficking compartment involved in arbuscular mycorrhizal symbiosis. *Front. Plant Sci.* **10**, 666. doi:10.3389/fpls.2019.00666

Bascom, C. S., Hepler, P. K. and Bezanilla, M. (2018). Interplay between ions, the cytoskeleton, and cell wall properties during tip growth. *Plant Physiol.* **176**, 28-40. doi:10.1104/pp.17.01466

Bravo, A., York, T., Pumplin, N., Mueller, L. A. and Harrison, M. J. (2016). Genes conserved for arbuscular mycorrhizal symbiosis identified through phylogenomics. *Nat. Plants* **2**, 15208. doi:10.1038/nplants.2015.208

Breakspear, A., Liu, C. W., Roy, S., Stacey, N., Rogers, C., Trick, M., Morieri, G., Mysore, K. S., Wen, J. Q., Oldroyd, G. E. D. et al. (2014). The root hair "infectome" of *Medicago truncatula* uncovers changes in cell cycle genes and reveals a requirement for auxin signaling in rhizobial infection. *Plant Cell* **26**, 4680-4701. doi:10.1105/tpc.114.133496

Camacho, C., Coulouris, G., Avagyan, V., Ma, N., Papadopoulos, J., Bealer, K. and Madden, T. L. (2009). BLAST plus : architecture and applications. *BMC Bioinformatics* **10**. doi:10.1186/1471-2105-10-421

Capella-Gutierrez, S., Silla-Martinez, J. M. and Gabaldon, T. (2009). trimAl: a tool for automated alignment trimming in large-scale phylogenetic analyses. *Bioinformatics* **25**, 1972-1973. doi:10.1093/bioinformatics/btp348

Cox, C. J. (2018). Land plant molecular phylogenetics: a review with comments on evaluating incongruence among phylogenies. *Crit. Rev. Plant Sci.* **37**, 113-127. doi:10.1080/07352689.2018.1482443

Curtis, M.D. and Grossniklaus, U. (2003). A gateway cloning vector set for high-throughput functional analysis of genes in planta. *Plant Physiol.* **133**, 462-469. doi:10.1104/pp.103.027979

Delaux, P.-M., Varala, K., Edger, P. P., Coruzzi, G. M., Pires, J. C. and Ané, J.-M. (2014). Comparative phylogenomics uncovers the impact of symbiotic

associations on host genome evolution. *PLoS Genet.* **10**, e1004487. doi:10.1371/journal.pgen.1004487

Delaux, P.-M., Radhakrishnan, G. V., Jayaraman, D., Cheem, J., Malbreil, M., Volkening, J. D., Sekimoto, H., Nishiyama, T., Melkonian, M., Pokorny, L. et al. (2015). Algal ancestor of land plants was preadapted for symbiosis. *Proc. Natl. Acad. Sci. USA* **112**, 13390-13395. doi:10.1073/pnas.1515426112

Doonan, J. H., Jenkins, G. I., Cove, D. J. and Lloyd, C. W. (1986). Microtubules connect the migrating nucleus to the prospective division site during side branch formation in the moss, *Physcomitrella patens*. *Eur. J. Cell Biol.* **41**, 157-164.

Edgar, R. C. (2004). MUSCLE: multiple sequence alignment with high accuracy and high throughput. *Nucleic Acids Res.* **32**, 1792-1797. doi:10.1093/nar/gkh340

Favre, P., Bapaume, L., Bossolini, E., Delorenzi, L., Falquet, L. and Reinhardt, D. (2014). A novel bioinformatics pipeline to discover genes related to arbuscular mycorrhizal symbiosis based on their evolutionary conservation pattern among higher plants. *BMC Plant Biol.* **14**, 333. doi:10.1186/s12870-014-0333-0

Feddermann, N. and Reinhardt, D. (2011). Conserved residues in the ankyrin domain of VAPYRIN indicate potential protein-protein interaction surfaces. *Plant Signal. Behav.* **6**, 680-684. doi:10.4161/psb.6.5.14972

Feddermann, N., Duvvuru Muni, R. R., Zeier, T., Stuurman, J., Ercolin, F., Schorderet, M. and Reinhardt, D. (2010). The *PAM1* gene of petunia, required for intracellular accommodation and morphogenesis of arbuscular mycorrhizal fungi, encodes a homologue of VAPYRIN. *Plant J.* **64**, 470-481. doi:10.1111/j.1365-313X.2010.04341.x

Finka, A., Saidi, Y., Goloubinoff, P., Neuhaus, J.-M., Zrÿd, J.-P. and Schaefer, D. G. (2008). The knock-out of *ARP3a* gene affects F-actin cytoskeleton organization altering cellular tip growth, morphology and development in moss *Physcomitrella patens*. *Cell Motil. Cytoskelet.* **65**, 769-784. doi:10.1002/cm.20298

Fournier, J., Timmers, A. C. J., Sieberer, B. J., Jauneau, A., Chabaud, M. and Barker, D. G. (2008). Mechanism of infection thread elongation in root hairs of *Medicago truncatula* and dynamic interplay with associated rhizobial colonization. *Plant Physiol.* **148**, 1985-1995. doi:10.1104/pp.108.125674

Genre, A., Chabaud, M., Timmers, T., Bonfante, P. and Barker, D. G. (2005). Arbuscular mycorrhizal fungi elicit a novel intracellular apparatus in *Medicago truncatula* root epidermal cells before infection. *Plant Cell* **17**, 3489-3499. doi:10.1105/tpc.105.035410

Genre, A., Chabaud, M., Faccio, A., Barker, D. G. and Bonfante, P. (2008). Prepenetration apparatus assembly precedes and predicts the colonization patterns of arbuscular mycorrhizal fungi within the root cortex of both *Medicago truncatula* and *Daucus carota*. *Plant Cell* **20**, 1407-1420. doi:10.1105/tpc.108.059014

Genre, A., Ivanov, S., Fendrych, M., Faccio, A., Žárský, V., Bisseling, T. and Bonfante, P. (2012). Multiple exocytotic markers accumulate at the sites of perifungal membrane biogenesis in arbuscular mycorrhizas. *Plant Cell Physiol.* **53**, 244-255. doi:10.1093/pcp/pcr170

Gutjahr, C. and Parniske, M. (2013). Cell and developmental biology of arbuscular mycorrhiza symbiosis. *Annu. Rev. Cell Dev. Biol.* **29**, 593-617. doi:10.1146/annurev-cellbio-101512-122413

Hanke, S. T. and Rensing, S. A. (2010). *In vitro* association of non-seed plant gametophytes with arbuscular mycorrhiza fungi. *J. Endocytobiosis Cell Res.* **20**, 95-101.

Harries, P. A., Pan, A. H. and Quatrano, R. S. (2005). Actin-related protein2/3 complex component ARPC1 is required for proper cell morphogenesis and polarized cell growth in *Physcomitrella patens*. *Plant Cell* **17**, 2327-2339. doi:10.1105/tpc.105.033266

Hemerly, A., Engler, J. D., Bergounioux, C., Vanmontagu, M., Engler, G., Inzé, D. and Ferreira, P. (1995). Dominant-negative mutants of the Cdc2 kinase uncouple cell division from iterative plant development. *EMBO J.* **14**, 3925-3936. doi:10.1002/j.1460-2075.1995.tb00064.x

Hepworth, J. and Lenhard, M. (2014). Regulation of plant lateral-organ growth by modulating cell number and size. *Curr. Opin. Plant Biol.* **17**, 36-42. doi:10.1016/j.pbi.2013.11.005

Hoang, D. T., Chernomor, O., von Haeseler, A., Minh, B. Q. and Vinh, L. S. (2018). UFBoot2: Improving the ultrafast bootstrap approximation. *Mol. Biol. Evol.* **35**, 518-522. doi:10.1093/molbev/msx281

Jensen, L. C. W. (1981). Division, growth, and branch formation in protonema of the moss *Physcomitrium turbinatum*: studies of sequential cytological changes in living cells. *Protoplasma* **107**, 301-317. doi:10.1007/BF01276832

Kalyaanamoorthy, S., Minh, B. Q., Wong, T. K. F., von Haeseler, A. and Jermiin, L. S. (2017). ModelFinder: fast model selection for accurate phylogenetic estimates. *Nat. Methods* **14**, 587. doi:10.1038/nmeth.4285

Katoh, K. and Standley, D. M. (2013). MAFFT multiple sequence alignment software version 7: Improvements in performance and usability. *Mol. Biol. Evol.* **30**, 772-780. doi:10.1093/molbev/mst010

Knight, C., Perroud, P.-F. and Cove, D. (2009). *The Moss Physcomitrella Patens*. Oxford, UK: Wiley-Blackwell.

Koenen, E. J. M., Ojeda, D. I., Steeves, R., Migliore, J., Bakker, F. T., Wieringa, J. J., Kidner, C., Hardy, O., Pennington, R. T., Herendeen, P. S. et al. (2019). The origin and early evolution of the legumes are a complex paleopolyploid phylogenomic tangle closely associated with the Cretaceous-Paleogene (K-Pg) boundary. *bioRxiv* 577957. doi:10.1101/577957

Kofuji, R. and Hasebe, M. (2014). Eight types of stem cells in the life cycle of the moss *Physcomitrella patens*. *Curr. Opin. Plant Biol.* **17**, 13-21. doi:10.1016/j.pbi.2013.10.007

Kofuji, R., Yagita, Y., Murata, T. and Hasebe, M. (2018). Antheridial development in the moss *Physcomitrella patens*: implications for understanding stem cells in mosses. *Philos. Trans. R. Soc. B Biol. Sci.* **373**, 20160494. doi:10.1098/rstb.2016.0494

Letunic, I. and Bork, P. (2019). Interactive Tree Of Life (iTOL) v4: recent updates and new developments. *Nucleic Acids Res.* **47**, W256-W259. doi:10.1093/nar/gkz239

Lev, S., Ben Halevy, D., Peretti, D. and Dahan, N. (2008). The VAP protein family: from cellular functions to motor neuron disease. *Trends Cell Biol.* **18**, 282-290. doi:10.1016/j.tcb.2008.03.006

Liu, C.-W., Breakspear, A., Stacey, N., Findlay, K., Nakashima, J., Ramakrishnan, K., Liu, M. X., Xie, F., Endre, G., de Carvalho-Niebel, F. et al. (2019). A protein complex required for polar growth of rhizobial infection threads. *Nat. Commun.* **10**, 2848. doi:10.1038/s41467-019-10029-y

Matasci, N., Hung, L.-H., Yan, Z. X., Carpenter, E. J., Wickett, N. J., Mirarab, S., Nguyen, N., Warnow, T., Ayyampalayam, S., Barker, M. et al. (2014). Data access for the 1,000 Plants (1KP) project. *Gigascience* **3**, 17. doi:10.1186/2047-217X-3-17

Menand, B., Calder, G. and Dolan, L. (2007). Both chloronemal and caulonemal cells expand by tip growth in the moss *Physcomitrella patens*. *J. Exp. Bot.* **58**, 1843-1849. doi:10.1093/jxb/erm047

Michaely, P., Machius, M., Tomchick, D. and Anderson, R. G. W. (2001). Structure of the ANK repeats of ankyrin. *Mol. Biol. Cell* **12**, 2477.

Mohler, P. J., Gramolini, A. O. and Bennett, V. (2002). Ankyrins. *J. Cell Sci.* **115**, 1565-1566.

Moody, L. A. (2019). The 2D to 3D growth transition in the moss *Physcomitrella patens*. *Curr. Opin. Plant Biol.* **47**, 88-95. doi:10.1016/j.pbi.2018.10.001

Murray, J. D., Duvvuru Muni, R. R., Torres-Jerez, I., Tang, Y., Allen, S., Andriankaja, M., Li, G., Laxmi, A., Cheng, X., Wen, J. et al. (2011). *Vapyrin*, a gene essential for intracellular progression of arbuscular mycorrhizal symbiosis, is also essential for infection by rhizobia in the nodule symbiosis of *Medicago truncatula*. *Plant J.* **65**, 244-252. doi:10.1111/j.1365-313X.2010.04415.x

Nguyen, L.-T., Schmidt, H. A., von Haeseler, A. and Minh, B. Q. (2015). IQ-TREE: a fast and effective stochastic algorithm for estimating maximum-likelihood phylogenies. *Mol. Biol. Evol.* **32**, 268-274. doi:10.1093/molbev/msu300

Okano, Y., Aono, N., Hiwatashi, Y., Murata, T., Nishiyama, T., Ishikawa, T., Kubo, M. and Hasebe, M. (2009). A polycomb repressive complex 2 gene regulates apogamy and gives evolutionary insights into early land plant evolution. *Proc. Natl. Acad. Sci. USA* **106**, 16321-16326. doi:10.1073/pnas.0906997106

Oldroyd, G. E. D., Murray, J. D., Poole, P. S. and Downie, J. A. (2011). The rules of engagement in the legume-rhizobial symbiosis. *Annu. Rev. Genet.* **45**, 119-144. doi:10.1146/annurev-genet-110410-132549

Ortiz-Ramírez, C., Hernandez-Coronado, M., Thamm, A., Catarino, B., Wang, M. Y., Dolan, L., Feijó, J. A. and Becker, J. D. (2016). A transcriptome atlas of *Physcomitrella patens* provides insights into the evolution and development of land plants. *Mol. Plant* **9**, 205-220. doi:10.1016/j.molp.2015.12.002

Perroud, P.-F. and Quatrano, R. S. (2008). *BRICK1* is required for apical cell growth in filaments of the moss *Physcomitrella patens* but not for gametophore morphology. *Plant Cell* **20**, 411-422. doi:10.1105/tpc.107.053256

Pfaffl, M. W. (2001). A new mathematical model for relative quantification in real-time RT-PCR. *Nucleic Acids Res.* **29**, e45. doi:10.1093/nar/29.9.e45

Prigge, M. J. and Bezanilla, M. (2010). Evolutionary crossroads in developmental biology: *Physcomitrella patens*. *Development* **137**, 3535-3543. doi:10.1242/dev.049023

Proust, H., Hoffmann, B., Xie, X. N., Yoneyama, K., Schaefer, D. G., Yoneyama, K., Nogue, F. and Rameau, C. (2011). Strigolactones regulate protonema branching and act as a quorum sensing-like signal in the moss *Physcomitrella patens*. *Development* **138**, 1531-1539. doi:10.1242/dev.058495

Pumplin, N., Mondo, S. J., Topp, S., Starker, C. G., Gantt, J. S. and Harrison, M. J. (2010). *Medicago truncatula* Vapyrin is a novel protein required for arbuscular mycorrhizal symbiosis. *Plant J.* **61**, 482-494. doi:10.1111/j.1365-313X.2009.04072.x

Pumplin, N., Zhang, X., Noar, R. D. and Harrison, M. J. (2012). Polar localization of a symbiosis-specific phosphate transporter is mediated by a transient reorientation of secretion. *Proc. Natl. Acad. Sci. USA* **109**, E665-E672. doi:10.1073/pnas.1110215109

Radhakrishnan, G. V., Keller, J., Rich, M. K., Vernié, T., Mbadinga Mbaginda, D. L., Vigneron, N., Cottret, L., San Clemente, H., Libourel, C., Cheema, J. et al. (2020). An ancestral signalling pathway is conserved in plant lineages forming intracellular symbioses. *Nat. Plants* **6**, 280-289. doi:10.1038/s41477-020-0613-7

Rich, M. K., Nouri, E., Courty, P.-E. and Reinhardt, D. (2017). Diet of arbuscular mycorrhizal fungi: bread and butter? *Trends Plant Sci.* **22**, 652-660. doi:10.1016/j.tplants.2017.05.008

Roth, R. and Paszkowski, U. (2017). Plant carbon nourishment of arbuscular mycorrhizal fungi. *Curr. Opin. Plant Biol.* **39**, 50-56. doi:10.1016/j.pbi.2017.05.008

Sakakibara, K., Nishiyama, T., Sumikawa, N., Kofuji, R., Murata, T. and Hasebe, M. (2003). Involvement of auxin and a homeodomain-leucine zipper I gene in

rhizoid development of the moss *Physcomitrella patens*. *Development* **130**, 4835-4846. doi:10.1242/dev.00644

Schaefer, D. G. (2002). A new moss genetics: Targeted mutagenesis in *Physcomitrella patens*. *Annu. Rev. Plant Biol.* **53**, 477-501. doi:10.1146/annurev.arplant.53.100301.135202

Schaefer, D. G. and Zrÿd, J.-P. (1997). Efficient gene targeting in the moss *Physcomitrella patens*. *Plant J.* **11**, 1195-1206. doi:10.1046/j.1365-313X.1997.11061195.x

Schaefer, D. G., Delacote, F., Charlot, F., Vrielynck, N., Guyon-Debast, A., Le Guin, S., Neuhaus, J. M., Doutriaux, M. P. and Nogué, F. (2010). RAD51 loss of function abolishes gene targeting and de-represses illegitimate integration in the moss *Physcomitrella patens*. *DNA Repair* **9**, 526-533. doi:10.1016/j.dnarep.2010.02.001

Schmiedel, G. and Schnepf, E. (1979). Side branch formation and orientation in the caulonema of the moss, *Funaria hygrometrica*: normal development and fine structure. *Protoplasma* **100**, 367-383. doi:10.1007/BF01279323

Smith, S. E. and Read, D. J. (2008). *Mycorrhizal Symbiosis*, 3rd edn. New York: Academic Press.

Thelander, M., Landberg, K. and Sundberg, E. (2018). Auxin-mediated developmental control in the moss *Physcomitrella patens*. *J. Exp. Bot.* **69**, 277-290. doi:10.1093/jxb/erx255

Trouiller, B., Schaefer, D. G., Charlot, F. and Nogue, F. (2006). MSH2 is essential for the preservation of genome integrity and prevents homeologous recombination in the moss *Physcomitrella patens*. *Nucleic Acids Res.* **34**, 232-242. doi:10.1093/nar/gkj423

Vidali, L., Rounds, C. M., Hepler, P. K. and Bezanilla, M. (2009). Lifeact-mEGFP reveals a dynamic apical F-actin network in tip growing plant cells. *PLoS ONE* **4**, e5744. doi:10.1371/journal.pone.0005744

Volkmar, U. and Knoop, V. (2010). Introducing intron locus cox1i624 for phylogenetic analyses in bryophytes: On the issue of *Takakia* as sister genus to all other extant mosses. *J. Mol. Evol.* **70**, 506-518. doi:10.1007/s00239-010-9348-9

Wang, B. and Qiu, Y.-L. (2006). Phylogenetic distribution and evolution of mycorrhizas in land plants. *Mycorrhiza* **16**, 299-363. doi:10.1007/s00572-005-0033-6

Waese, J., Fan, J., Pasha, A., Yu, H., Fucile, G., Shi, R., Cumming, M., Kelley, L.A., Sternberg, M. J., Krishnakumar, V. et al. (2017). ePlant: Visualizing and exploring multiple levels of data for hypothesis generation in plant biology. *Plant Cell* **29**, 1806-1821. doi:10.1105/tpc.17.00073

Wang, W., Shi, J., Xie, Q., Jiang, Y., Yu, N. and Wang, E. (2017). Nutrient exchange and regulation in arbuscular mycorrhizal symbiosis. *Mol. Plant* **10**, 1147-1158. doi:10.1016/j.molp.2017.07.012

Wu, S.-Z., Ritchie, J. A., Pan, A.-H., Quatrano, R. S. and Bezanilla, M. (2011). Myosin VIII regulates protonemal patterning and developmental timing in the moss *Physcomitrella patens*. *Mol. Plant* **4**, 909-921. doi:10.1093/mp/ssr068

Wu, S.-Z., Yamada, M., Mallett, D. R. and Bezanilla, M. (2018). Cytoskeletal discoveries in the plant lineage using the moss *Physcomitrella patens*. *Biophys. Rev.* **10**, 1683-1693. doi:10.1007/s12551-018-0470-z

Zhang, X. C., Pumplin, N., Ivanov, S. and Harrison, M. J. (2015). EXO70I is required for development of a sub-domain of the periarbuscular membrane during arbuscular mycorrhizal symbiosis. *Curr. Biol.* **25**, 2189-2195. doi:10.1016/j.cub.2015.06.075